



EXPERIMENTAL ASSESSMENT OF THE CYCLIC BEHAVIOR OF PERUVIAN CONFINED MASONRY WALLS AND NUMERICAL MODELING USING GENETIC ALGORITHMS

L. G. Quiroz⁽¹⁾, Y. Maruyama⁽²⁾, C. Zavala⁽³⁾

⁽¹⁾ Associated Researcher, Department of Earthquake Engineering, Japan-Peru Earthquake Engineering and Disaster Mitigation Center, Faculty of Civil Engineering, National University of Engineering, Lima-Peru, lgquiroz@uni.edu.pe.

⁽²⁾ Associate Professor, Department of Urban Environment Systems, Chiba University, Japan, ymaruyam@faculty.chiba-u.jp.

⁽³⁾ Researcher, Japan-Peru Earthquake Engineering and Disaster Mitigation Center, Faculty of Civil Engineering, National University of Engineering, Lima-Peru, czavala@amauta.rcp.net.pe.

Abstract

In Peru, confined masonry (CM) walls are widely used as structural elements in low- and mid-rise dwellings in order to resist the gravity and seismic loads. To evaluate the seismic capacity, test results of four full-scale specimens subjected to cyclic load are presented and analyzed. The specimens were constructed with solid handmade clay bricks and lime mortar. The dimensions of all the specimens were kept constant while the reinforcement ratio of the bond beam and tie-columns were changed. The structural behaviors of the specimens were studied in terms of strength, lateral stiffness, dissipated energy, and equivalent viscous damping. Then, a macro-model based on an equivalent strut approach that considers a smooth hysteretic model was calibrated and validated in order to reproduce the behaviors of some specimens. The genetic algorithm (GA) that considered the experimental results was employed to develop the numerical model. The parameters obtained from the calibration process were applied to the other CM walls to evaluate their applicability. The results obtained from the numerical simulations and the experiments showed good agreements. The calibrated model can be used to assess the seismic behaviors and estimate damage to existing structures.

Keywords: Confined masonry wall, Full-scale test, Genetic algorithms.



1. Introduction

One of the most widely used materials for the walls of dwellings in Peru is masonry, especially in Lima. This kind of material is used in both urban and rural areas for low- and mid-rise dwellings due to the low cost compared with other structural systems (e.g., RC frames and RC walls). Masonry walls are usually constructed in two ways, confined masonry (CM) and reinforced-concrete (RC) frames with masonry infill. CM walls are composed by an unreinforced masonry panel confined with RC tie-columns and bond-beams. CM walls are structural elements in charge of taking gravitational and seismic lateral loads. This type of construction seems to have more strength, ductility, and stiffness than unreinforced masonry walls, and it showed better seismic performance during recent earthquakes.

The last big earthquake that occurred in Peru was the Pisco earthquake in August 15, 2007 ($M_w = 8.0$), which caused severe damage to masonry constructions. However, the last big earthquake that hit Lima occurred in 1974. It is expected that masonry dwellings that were properly built according to the requirements of design standard for masonry structures [1] will show good seismic performance.

Around the world, many studies have been conducted on complete structures or structural elements in order to increase the understanding of the behavior of masonry walls or to improve standards. Those studies have considered variations in the characteristics of materials or configurations of the components. For example, Tena-Colunga et al. [2] found that combined and CM walls jointed with non-engineered mortar did not satisfy all the criteria to be qualified as earthquake resistant walls. On the other hand, the combined and CM walls jointed with engineered mortar showed a performance (cracking patterns, initial stiffness, cracking drift angle, drift angle for design, etc.) equivalent to the experimental results for similar CM walls made with solid clay bricks. In other study, Torrisi et al. [3] observed that a separation occurs between the masonry panel and the confining elements at initial stages of loading for both CM and infill walls. They also found a formation of a compression stress field in a masonry panel using experimental data and numerical simulations. In 2008, Salinas and Lazares [4] studied the seismic performance and improvement of structural performance of CM walls with hollow and tubular brick units.

Despite the many experimental studies conducted in Peru and other countries, the behavior of CM walls is still not well known [5], and the results tend to be for the characteristics of structural systems related to regional situations (e.g., construction process, quality of labor, material properties). The available information of studies on CM walls in Peru is limited. Hence, continuing with the experimental study of CM walls in countries where they are widely used like in Peru is important. For the present study, the experimental results of test on CM walls carried out at CISMID in Lima, Peru [6] will be analyzed using their structural characteristics and a numerical simulation. Then, based on test results, an equivalent strut approach with a smooth hysteretic model is calibrated using a genetic algorithm procedure and the validation of the numerical simulation is discussed.

2. Outline of the experiments

Four walls were constructed and tested under cyclic lateral loading. Two groups of walls were considered, with each group containing two specimens. The first group was called A1, and the specimens were named A1-1 and A1-2. Similar denominations were used for the second group. The difference between A1-1 and A1-2 was the reinforcement ratio used in the bond beams while the difference between A2-1 and A2-2 was the reinforcement ratio of the tie-columns. The transversal reinforcement of the confining elements was kept constant for all walls. The geometry of the walls is schematically shown in Fig. 1. The general dimensions of the specimens were set to be as close as possible to the dimensions of a CM wall used in low- and mid-rise dwellings.

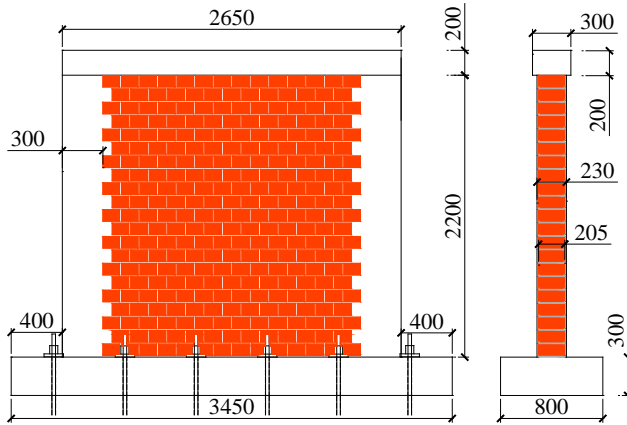


Fig. 1. General geometry of specimens

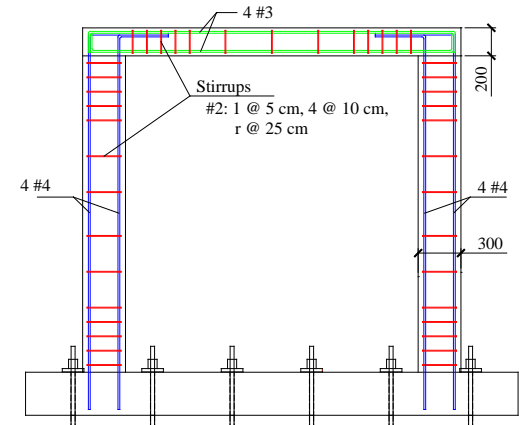


Fig. 2. Reinforcement of confining elements in specimen A1-1

The specimens were monolithically connected to the foundation. The characteristics of the confining elements with the reinforcement are presented in Table 1. Figure 2 shows the reinforcement's arrangement (longitudinal and transversal reinforcement) in the confining elements for specimen A1-1. Reinforcement distribution in other specimens were similar. The compressive strength of the concrete used for the confining tie-columns and bond beams was 20.6 MPa.

Handmade brick units made from clay were used in the specimens. The brick units did not present holes in the bed area. They are usually used in expansion areas of the urban zones in Lima, and they do not have good resistance compared to factory-made brick units. A set of five masonry prisms was constructed to define the compressive strength (f'_m) and Young's modulus (E_m) for the masonry. The value of f'_m was 3.74 MPa. Both bed and head joints were filled with 10 mm thick mortar. The mortar was measured by volume using a 1:4 cement-coarse sand proportion. The values of f'_m and E_m were estimated following the requirements of the current standard E.070 [1]. The value of E_m was estimated as $500 f'_m$ given a value of 1870 MPa. Because of the lack of diagonal compression tests for low walls, the shear resistance (v'_m) was set to 0.5 MPa, as suggested in the design standard [1]. This decision was made because the value of f'_m obtained from test was very close to that suggested by the masonry design standard for handmade bricks.

Table 1. Dimensions and reinforcements of walls and confining elements.

Specimen	Masonry			Tie-column			Bond beam		
	L (mm)	t (mm)	H (mm)	t (mm)	b (mm)	Longitudinal Reinforcement	h (mm)	b (mm)	Longitudinal Reinforcement
A1-1						4 #4 ^a			4 #3
A1-2	2650	205	2200	230	300	4 #4	200	300	4 #4
A2-1						4 #3 ^b			4 #3
A2-2						4 #4			4 #3

^a 4 #4: Four conventional rebars, 12.7 mm in diameter, in the section of the element.

^b 4 #3: Four conventional rebars, 9.5 mm in diameter, in the section of the element.

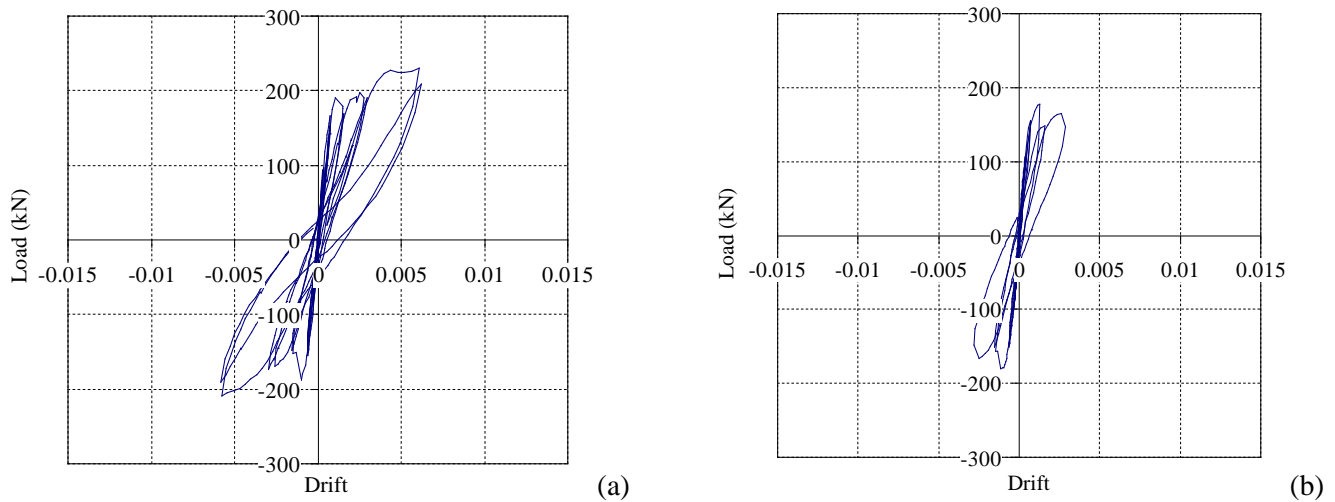


Fig. 3. Overall hysteretic responses of walls: (a) A1-1, and (b) A2-1

The specimens were instrumented with force transducers and displacement transducers (LVDTs) to monitor the loads and in-plane displacements. Prior to the application of the lateral load, a vertical load of approximately 78.45 kN was applied. This load represented the weight that should be expected at the bottom of a central wall in a two-story building, and it was kept constant throughout the tests.

Compared to other countries like Mexico [2], Peru has no regulations on the protocol for testing CM walls. Therefore, in order to simulate the loading expected during an earthquake, a simple horizontal cyclic loading history with small increments was applied at a quasi-static rate with the cycles controlled by the displacement. The horizontal load was applied at the center of the bond beam at the top of the wall. The loading history consists of six phases, and every phase was repeated two times (two cycles). The target drifts for every phase were 1/3200, 1/1600, 1/800, 1/400, 1/200 and 1/100 with target top displacements of 0.75, 1.51, 3, 6, 12 and 24 mm, respectively. The exceptions were specimens A1-1 and A2-1, which were only tested for five and four phases, respectively, because of problems with the displacement transducers.

Figure 3 shows the relationships between the applied load and the ratio of top displacement to height (drift) of the walls A1-1 and A2-1 obtained from test. The hysteretic loops seem to be symmetric and stable for positive and negative cycles up to a drift of 0.005. All the hysteretic curves present the same level of pinching and unloading stiffness.

With regard to the cracking of the elements, most of the specimens presented cracks at the backs of the tie-columns in phase 1 (flexure effect on the confining elements). In phase 2, the cracks in the bottoms of the columns became more serious. The number of cracks in the tie-columns increased in phase 3 along the height of the confining element, and the first shear cracks on the panel appeared. The shear cracks propagated in phase 4, and they were found almost everywhere along the diagonal of the wall in phase 5. Two of the walls presented spalling in part of the bricks, and one of them presented crushing in a corner. The experimental results for wall A1-1 were used in this study to calibrate the parameters of the numerical model, and then those values were verified using the results for the other walls.

3. Evaluation of structural characteristics of CM walls based on experiments

4.1 Maximum strength of walls

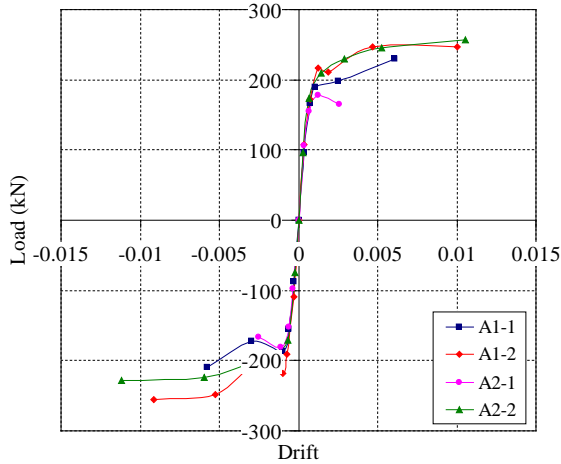


Fig. 4. Skeleton curves for all specimens

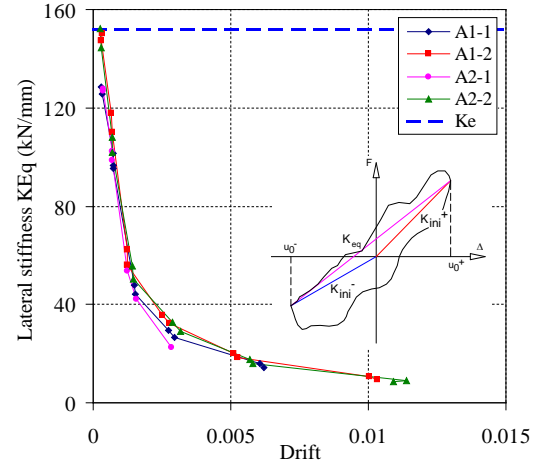


Fig. 5. Variation of lateral equivalent stiffness

Figure 4 shows skeleton curves (obtained from peak lateral loads from the hysteretic curves) estimated from the experimental results for all the specimens. The behaviors of the walls in the elastic range are similar for a drift smaller than 0.0007. The responses of the specimens in the inelastic range are slight different. Specimens A1-2 and A2-2 present the largest maximum strengths. Specimen A2-1 exhibits the lowest value because the associated drift of this specimen was also the smallest applied.

4.2 Initial stiffness and stiffness degradation

The initial stiffness before cracking is calculated using Eq. (1)

$$K = \frac{1}{\left(\frac{h_w^3}{3E_m I} + \frac{h_w}{G_m A_v} \right)} \quad (1)$$

where E_m is the elastic modulus of masonry, and G_m is the shear modulus of masonry (defined as $0.40 E_m$ in [1]). A_v is the shear area, and I is the moment of inertia of the transformed section. The initial stiffness for all the specimens is 151.64 kN/mm.

Figure 5 shows the variation of lateral equivalent stiffness (K_{eq}) with respect to the drift for all specimens. The results are rather similar among the four specimens. It is observed that there are no significant differences between the curves of the first and second cycles for all the specimens. The lateral stiffness is less than 40% of its initial value for a drift of 0.00125. At drift limit (drift = 0.005) established by the Peruvian code [7], the lateral stiffness reduced to 15% of the initial value. When the specimens reached a 93% reduction of the initial stiffness, the spalling of the masonry started.

4.3 Dissipated energy and equivalent viscous damping

Figure 6 shows the cumulative dissipated energy as a function of the drift obtained from the area under the hysteretic curves [8]. All the specimens exhibit almost the same amount of dissipated energy in every cycle. For the first two phases, a very small amount of energy was dissipated.

Another term to analyze the energy dissipation is damping. For structural elements under cyclic loads, it is common to use the equivalent viscous damping (ξ_{eq}) defined in Eq. (2) [8].

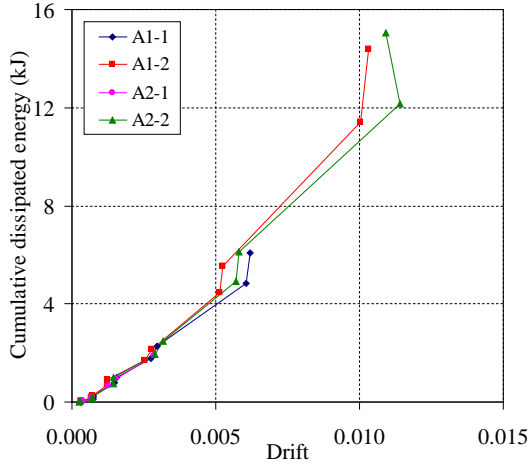


Fig. 6. Cumulative dissipated energy versus drift

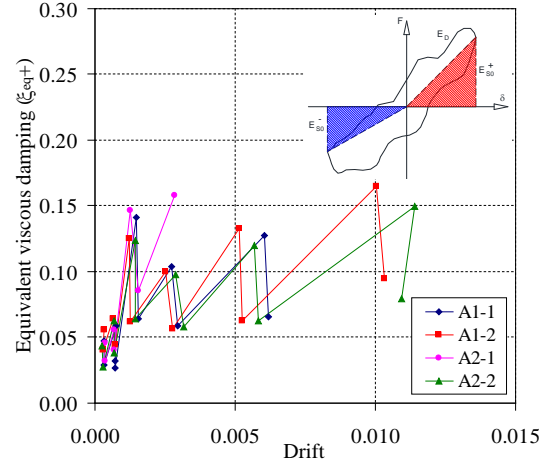


Fig. 7. Equivalent viscous damping versus drift

$$\xi_{eq} = \frac{1}{4\pi} \left(\frac{E_D}{E_{S0}} \right) \quad (2)$$

where E_D is the dissipated energy in one cycle, and E_{S0} is the elastic strain energy stored in an equivalent linear elastic system at the maximum displacement. Figure 7 shows the equivalent viscous damping, which is derived using the positive part of the cycle, in terms of the drift. The equivalent viscous damping during the first two phases is approximately 0.05 for all the specimens. This value increases on average to 0.10 for a drift of 0.005.

5. Calibration of equivalent strut model with smooth hysteretic model using GA for CM walls

Numerical models of specimens are prepared and calibrated using the test results, and IDARC 2D version 7 [9] is employed in this study. Equivalent strut model with smooth hysteretic model is used to simulate the nonlinear response under cyclic loading for masonry panel. The required parameters to define the hysteretic model are calibrated using the results of the wall A1-1 using GA. The parameters are validated with the results of the other walls.

5.1 Numerical modeling of specimens

Torresi et al. [3] established that the responses of CM walls and masonry infill walls to inplane loads are somewhat similar, because the behavior of the system is controlled by the nonlinear response of the masonry wall panels and the surrounding RC elements. Therefore, these structural systems can be analyzed using similar models. The masonry panels were represented as macro-models (i.e., compression strut elements) with a smooth hysteretic model for the two diagonals of the panel. The individual masonry struts are considered ineffective in tension. The existence of the two diagonals struts provides lateral resistance to cyclic loading (Fig. 8(a))

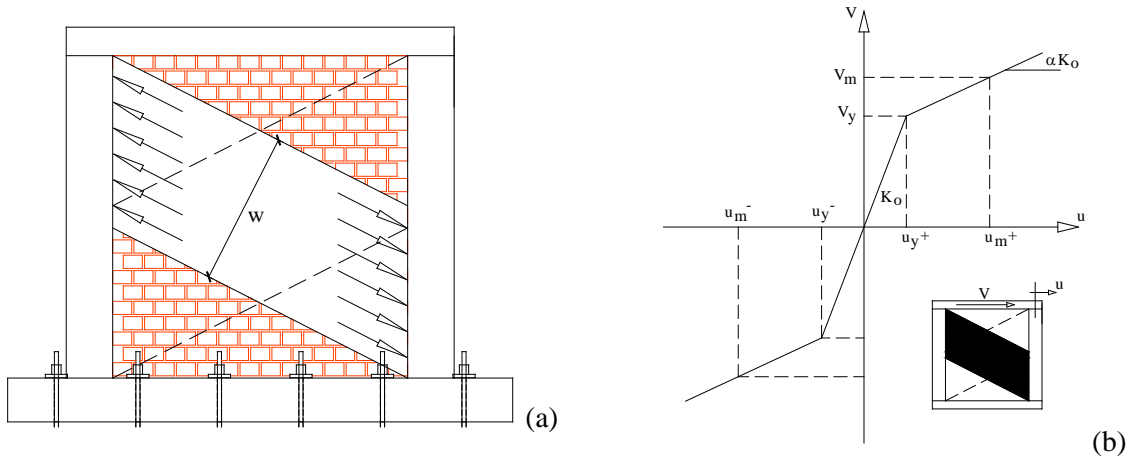


Fig. 8. (a) Equivalent strut model for masonry panels and (b) Strength envelope for masonry panels [9]

The lateral force–deformation relationship for the structural masonry is assumed to be a smooth curve bounded by a linear strength envelope with an initial elastic stiffness until a yield force V_y , and there on a post-yield degraded stiffness until the maximum force V_m is reached. (Fig. 8(b)). An initial elastic stiffness of the panel (K_o) and a lateral yield force of the panel (V_y) define the initial behavior of the strut. K_o was estimated considering Eq. (3):

$$K_o = E_m * A / L \quad (3)$$

where E_m is the modulus of elasticity of masonry, and A and L are the area and length of the equivalent strut, respectively. The area of the strut can be estimated as

$$A = w * t \quad (4)$$

where w is the width of the strut, and t is the thickness of the wall. For the estimation of w , the definition of Bazan and Meli [10] was employed. The yield force V_y was estimated according to current E.070 [1].

Tie-column elements were considered as macro-elements with inelastic flexural deformations, and elastic shear and axial deformations while bond beams elements were modeled using a nonlinear flexural stiffness model and linear elastic shear deformations. The hysteretic response of a section was traced using a three-parameter model that considered a trilinear polygonal skeleton, along with the stiffness degradation, strength deterioration, and pinching response considering a moderate degrading of the elements [9]. Confined concrete was assumed, and the Kent and Park model was employed. The tensile strength of concrete was neglected. The uniaxial behavior of the reinforcement was modeled using the trilinear model. The behaviors are considered to be the same for compressive and tensile stresses.

The smooth hysteretic model assumed in this study is based on the Sivaselvan and Reinhorn model [11]. This model is based on a smooth hysteretic force–displacement relationship. The hysteretic model includes the effects of stiffness degradation, strength deterioration, and pinching, and it is based on 12 parameters defining the: (a) smooth hysteretic model ($A, \beta, \gamma, n, \alpha$), (b) stiffness degradation (S_k), strength degradation ($S_{p1}, S_{p2}, \mu_{max}$), and slip-lock behavior (A_s, Z, \bar{Z}). Details about the hysteretic model can be found in [9].

5.2 Process of calibration based on genetic algorithm (GA)



A genetic algorithm (GA) is an optimization process inspired by Darwin's theory of evolution. GA has recently been applied to the field of structural engineering, e.g., Wang and Ohmori [12] employed a layered GA in order to optimize the structural design of truss by taking into consideration their ultimate load-carrying capacity.

The current research uses a simple form of GA for the hysteretic parameter calibration which considers the following steps: definition of a population, encoding, initial population, reproduction, crossing, mutation, generation of new populations, and testing of convergence. In the definition of the population and encoding, each parameter of the hysteretic model is binary encoded to represent a gene. Five-bit long gene was considered. The union of several genes forms an individual. Each individual represents a point in the search space. A group of N_i individuals in the i -th generation defines the population. The initial population N_0 is randomly generated in the search space. Then, the mechanisms of selection, reproduction, and mutation are employed to evolve the population to the best individuals in the search space. For reproduction and crossing, the parents are duplicated and then randomly paired while being careful not to match the same parents. Then, we cross over to generate new pairs of offspring by exchanging part of the genes. The locations of the crossover points are chosen randomly. Some offspring are randomly mutated by changing the code of one bit of one gene in order to limit the convergence problems and diversify the population. The selections of the individual and the gene to be mutated are performed randomly. The probability of mutation is set to 0.005. This is the final population, and is called a new population. Finally, an error function is evaluated for the new population. The previous steps are repeated until the error function of the new generation is less than a given error or until a limited number of generations is reached. This process was repeated for five trials in this study.

The error function for each individual of the population is evaluated using Eq. (5)

$$E.I. = \left(\sum_{j=1}^4 e_j \right) / 4 \quad (5)$$

where e_j is the relative error of a structural characteristic based on the hysteretic curves (i.e., strength, stiffness degradation, cumulative dissipated energy, and unloading stiffness). The relative error of a structural characteristic is defined as

$$e_j = \left(\frac{\sum_{k=1}^r (Y_{test} - Y_{sim})^2}{\sum_{k=1}^r Y_{test}^2} \right)^{1/2} \quad (6)$$

where Y_{test} is the structural characteristic obtained from the test, Y_{sim} is the structural characteristic obtained from the numerical simulation, and r is the number of referenced points of the structural characteristics.

To start the analysis, range values were set for the parameters as follow: $A = [0.5-1.5]$, $\beta = [0.001-0.6]$, $\gamma = [0.5-1.6]$, $n = [2-4]$, $\alpha = [0.01-0.05]$, $S_k = [0.1-5]$, $S_{p1} = [0.001-1.6]$, $S_{p2} = [0.5-1.5]$, $\mu_{max} = [45-55]$, $A_s = [0.015-0.4]$, $Z = [0.01-0.5]$, and $\bar{Z} = [-0.1-0.3]$. A value of 20 was set for the number of individuals per generation. The smallest E.I. among these 20 individuals was regarded as the best solution in every generation. Then, the variations in the parameters with respect to the number of generations were evaluated. Figure. 9 shows the variation of parameters A and α with number of generations. It can be observed that parameter A tends to present a value between 0.75 and 1.1 while Parameter α tends to have values larger than 0.03. Some parameters did not show clear tendencies.

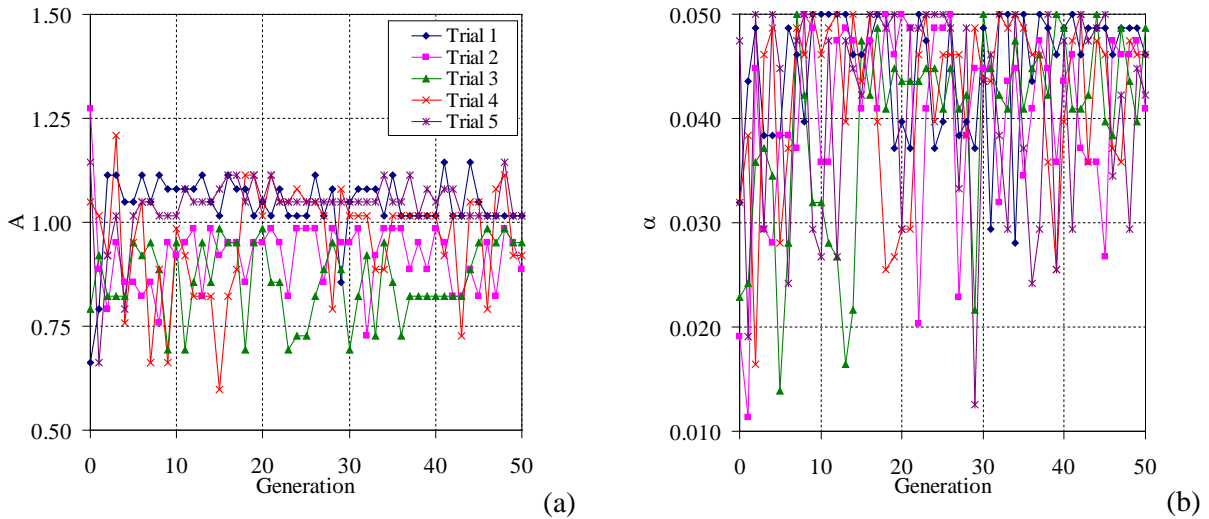


Fig. 9. Variations in values of parameters with respect to number of generations (first analysis)

These findings led us to reallocate the search space of the parameters and a second analysis was performed. For parameters A and S_k , the search space was narrowed, whereas the search space was extended for the other parameters. Based on these two analyses, it was inferred that those parameters that did not present clear tendencies had little influence on the structural characteristics. Then, a third analysis was carried out, assuming constant values for these parameters, following those in reference [9]. New ranges of values were assigned for parameters $A = [0.75-0.9]$, $\alpha = [0.04-0.065]$, $A_s = [0-0.4]$, and $S_k = [0.5-1.5]$, based on the previous analysis. Figure 10 shows the variation of the smallest E.I. with respect to the number of generations in the third analyses.

Table 2 lists the parameters associated with the smallest E.I. for every trial. All of the estimated parameters presented a low coefficient of variation (C.V.), except for the parameter A_s .

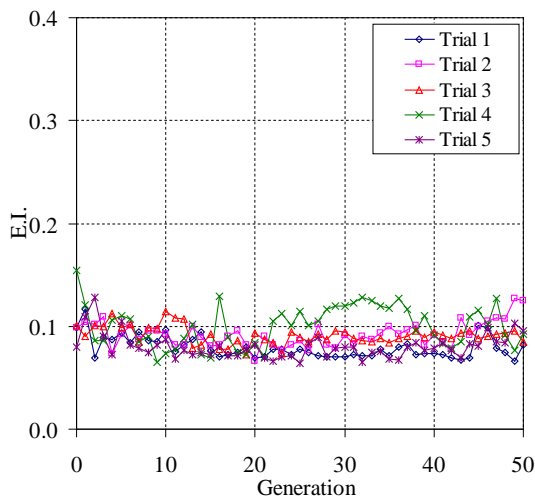


Fig. 10. Variations in smallest E.I. with respect to number of generations for third analysis

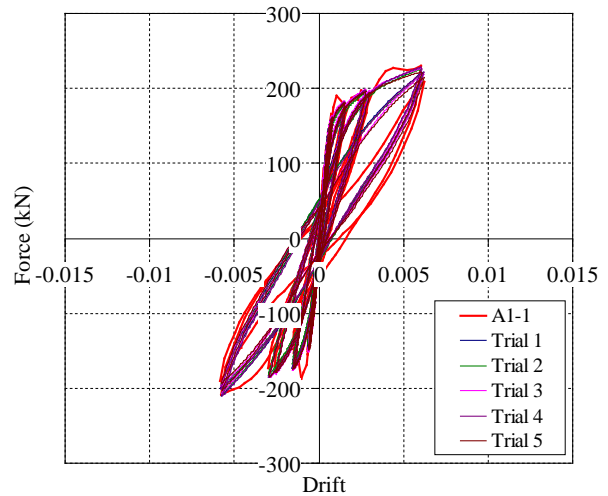


Fig. 11. Comparisons of experimental results with numerical simulation for wall A1-1: hysteresis curve

Table 2. Mean value and coefficient of variation for best solutions of parameters (third analysis)

Trial	Parameters				
	A	n	α	As	S _k
Mean	0.836	4.142	0.044	0.005	1.145
C.V. (%)	3.154	8.975	3.770	136.931	4.454

Figure 11 compares the response from the numerical simulation using the estimated parameters with the experimental results of wall A1-1. The results of the numerical simulation show good agreement with those of the experiment in terms of the hysteretic curve and also strength, stiffness degradation, cumulative dissipated energy dissipated, and unloading stiffness.

5.3 Validation of parameters based on results for other walls

The applicability of the mean values presented in previous section is evaluated using the results from other walls. The validation was performed by comparing the same structural characteristics presented in section 4.

Figure 12 shows a comparison between the hysteretic curves obtained from the numerical simulation and the test for the walls A1-2 and A2-1. As can be observed, the hysteretic curves obtained from the numerical simulation show good estimations of those obtained from the experimental results, especially for a drift smaller than 0.006. The structural characteristics (i.e., strength, stiffness degradation, cumulative dissipated energy, and unloading stiffness) obtained from the hysteretic curves also show good correlations.

6. Conclusions

Test results of four full-scale CM walls subjected to cyclic loads were presented and analyzed in terms of structural characteristics. The values of the parameters that define a smooth hysteretic model for masonry panels were calculated based on GA technique and experimental results of one wall. Then, the values were validated using the experimental results of other walls. The following conclusions can be drawn:

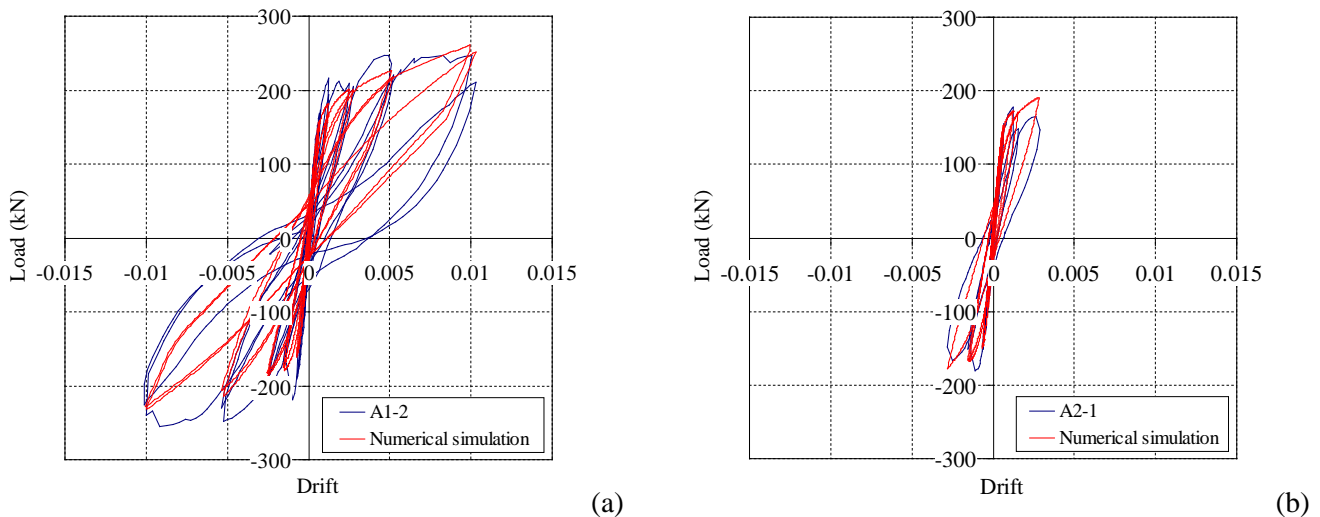


Fig. 12. Comparison of simulated and experimental hysteretic curves for walls: a) A1-2, c) A2-1, and c) A2-2



The CM walls presented different amounts of reinforcement in the confining elements but most of their structural characteristics showed similar tendencies in terms of the strength, stiffness degradation, energy dissipated, and equivalent viscous damping. That fact indicates that the behavior of the specimens was mainly governed by the characteristics of the masonry panel. No clear strength degradation was observed for all specimens. Only the wall with the lowest reinforcement ratios for the bond beams and tie-columns presented a slight reduction in the maximum strength and lateral stiffness. The structural characteristic that exhibited more dispersion was the equivalent viscous damping.

Twelve parameters were used to model the hysteretic behavior of the masonry panel. The mean values of the parameters were calibrated using a GA technique founding the values of 0.836, 4.142, 0.044, 0.005, and 1.145, for the parameters A , n , α , A_s , and S_k , respectively. The parameters β , γ , Z , \bar{Z} , S_{p1} , S_{p2} , and μ_{max} did not show clear tendencies indicating that they had small influences on the structural characteristics evaluated.

Even though the number of specimens analyzed is limited, the comparisons between the experimental data and the simulated results indicated good agreement in this research. Nevertheless, more test results are still required. The results of the numerical simulation are in good agreement with the experimental results validating the proposed values in the case of CM walls. The calibrated model will be used to evaluate the seismic performance of CM structures using fragility curves.

7. References

- [1] SENCICO (2006): *Standard E.070 masonry*. National Building Regulations, Lima, Peru. (In Spanish).
- [2] Tena-Colunga A, Juarez-Angeles A and Salinas-Vallejo V (2009): Cyclic behavior of combined and confined masonry walls. *Engineering Structures* **31**, 240-259.
- [3] Torrisi GS, Crisafulli FJ and Pavese A (2012): An innovative model for the in-plane nonlinear analysis of confined masonry and infilled frame structures. *Proceedings of 15th World Conference on Earthquake Engineering*, Lisbon, Portugal. Paper No 0574.
- [4] Salinas R and Lazares F (2008): Seismic performance of confined masonry buildings with tubular bricks in developing areas. *Proceedings of 14th World Conference on Earthquake Engineering*, Beijing, China. Paper No. 05-04-0003.
- [5] Yañez F, Astroza M, Holmberg A and Ogaz O (2004): Behavior of confined masonry shear walls with large openings. *Proceedings of the 13th World Conference on Earthquake Engineering*, Vancouver, B.C., Canada. Paper No 3438.
- [6] Zavala C, Honma C, Gibu P, Gallardo J and Huaco G (2004): Construction, monitoring and improvement techniques for masonry housing CISMID/FIC/UNI. *Research Report. Japan-Peru Center for Earthquake Engineering Research and Disaster Mitigation*. Lima, Peru (in Spanish).
- [7] SENCICO (2003): *Standard E.030 seismic design*. National Building Regulations, Lima, Peru. (In Spanish)
- [8] Chopra A (2012): *Dynamic of structures—Theory and applications to earthquake engineering*. Pearson Prentice Hall, New Jersey. Third Edition.
- [9] Reinhorn AM, Roh H, Sivaselvan M, Kunnath SK, Valles RE, Madan A, Li C, Lobo R and Park YJ (2009): IDARC2D version 7.0: A program for the inelastic damage analysis of structures. *Technical Report MCEER-09-0006*, State University of New York at Buffalo.
- [10] Bazan M and Meli R (2009): *Seismic design of buildings*. Limusa Noriega Ed. Mexico. (In Spanish).
- [11] Sivaselvan MV and Reinhorn AM (1999): Hysteretic models for cyclic behavior of deteriorating inelastic structures. *Technical Report NCEER-99-0018*, National Center for Earthquake Engineering Research, Dept. of



Civil, Structural and Environmental Engineering, University at Buffalo, The State University of New York, Buffalo, NY.

- [12] Wang H and Ohmori H (2013): Elasto-plastic analysis based truss optimization using Genetic Algorithm. *Engineering Structures* **50**, 1–12.